DFT Comparison the Performance of $Pd_{10}Sn_5$ and $Pd_{10}Ag_5$ Electrocatalyst for Reduction of CO_2

Yu Han, Zhijia Zhang[#], Xinyi Guo, Minmin Xing, Ling Guo*

School of Chemistry and Material Science, Key Laboratory of Magnetic Molecules and Magnetic Information Materials, Ministry of Education, Shanxi Normal University, Linfen 041004, China

Abstract: CO_2 electrocatalysis as a hydrocarbon is a promising means of achieving economical CO_2-mediated hydrogen energy cycling. Hydrocarbons are renewable hydrogen storage materials. The development of reliable metal alloy electrocatalysts is an urgent but challenging task associated with such systems, although there is still a lack of precise reaction mechanism design. In this study, the performance of $Pd_{10}Ag_5$ alloy nanoparticles (NPs) and $Pd_{10}Sn_5$ alloy nanoparticles (NPs) on the electrocatalytic reaction of CO_2 was compare. The kinetic and density functional theory (DFT) calculations show that the selectivity of the Pd-based bimetallic catalyst to the C2 product is greater than that of C1, and the stability of $Pd_{10}Ag_5$ is better and less affected by the reaction environment. However, the catalytic performance of the $Pd_{10}Sn_5$ electrocatalyst in the liquid phase is the best. The insight obtained from the calculations is used to develop criteria for identifying new and improved catalysts for electrochemical CO_2 reduction.

Key words: $Pd_{10}Sn_5$; $Pd_{10}Ag_5$; electrocatalysts; CO_2 conversion; Reaction Mechanism; DFT

1. Introduction

The emission of carbon dioxide (CO_2) has been at record levels, and it is expected to rise higher in future decades due to the accelerated consumption of fossil fuels.[1-3] The development of CO_2 conversion technologies is imperative to successfully recycle the anthropogenically emitted greenhouse gas to produce future carbon resources of fuels and chemicals. Utilization of renewable energy sources to convert CO_2 into value-added chemicals and fuels is an attractive strategy to not only mitigate the excess CO_2 levels in the atmosphere, but also to convert renewable electricity into energy-dense liquid forms that are convenient for storage and

*Corresponding author：Ling Guo

E-mail address: jisuanhuaxue0@163.com

1 transportation.[4-6] Electrochemical reduction of CO_2 (ERC) under mild conditions provides an

2 alternative protocol to producing industrial feedstock chemicals with intermittent renewable

3 electricity sources (electricity generated by solar, wind, tide, etc.). Comparing to conventional

4 chemical processes, ERC provided a "clean" and efficient way to mitigate energy shortage and to

5 lower the global carbon footprint. [7-10] Electrochemical CO_2 conversion is considered one of the

6 most feasible and promising technologies because of its high reactivity under ambient conditions,

7 its wide product window according to the type of catalyst, and its applicability in commercial

8 processes. Thus, many experimental and theoretical studies have extensively developed

9 high-performance electrochemical catalyst systems for CO_2 conversion to achieve a minimized

10 overpotential, improved product selectivity, improved stability, etc.[11-14] And CO_2 is reduced to

11 various products based on a multielectron transfer mechanism.[15,16] The main target products are

12 often classified into C1 product (e.g., CO, CH_4, CH_3OH, and HCOOH, etc.) and C2 product (e.g.,

13 C_2H_4, C_2H_5OH, and CH_3COOH, etc.). To produce longer chain chemicals or fuels (i.e. >C1)

14 during the electrocatalytic reduction of CO_2 is a great challenge, but rather interesting from the

15 application perspective: better use as drop-in products, better sustainability with respect to the

16 multistep current production.[17] Therefore, the development of catalysts with appropriate electronic

17 properties becomes critical and more industrially desirable for tuning the selectivity for C2

18 products.

19   However, electrochemical CO_2 reduction techniques for producing fuels are still not

20 mature enough for commercialization. Most metal catalysts produce predominantly single carbon

21 products (i.e., C1 products: CO, CH_4, CH_3OH, HCOOH), and only Cu is known to convert CO_2 to

22 C2+ products with moderate selectivity. In order to promote the electrocatalysis of C2+ products,

23 it is necessary to develop strategies and materials that have desirable reaction intermediate binding

24 energies, promote carbon-carbon bond formation, and are kinetically beneficial to the desired

25 reaction pathway rather than possible side reactions. Compared to conventional bulk metal

26 electrodes, nanoparticle electrocatalysts have greater surface to volume/mass ratios[18] and allow

27 precise control of size, composition, atomic structure and morphology,[19,20] which typically results

28 in higher electrochemical CO_2 reduction performance.

29   In this context, Bimetallic catalysts are currently the most promising for driving CO_2RR to

30 produce significant amounts of multicarbon oxygenates and hydrocarbons.[21] Adding a second

metal can be an effective strategy to tune catalytic performance through modification of electronic and structural factors[22] or via a bifunctional effect in which atoms of the two metals provide catalytic sites which play unique roles, such as separating the adsorption of different reactants or intermediates.[23]

Recently, Pd based catalysts, which have a high oxygen adsorption ability and a lower cost than Pt- and Rh-based catalysts, have attracted considerable attention, for example, as a replacement for the expensive catalysts used to remove CO from vehicle exhaust.[24,25] Specically, alloying Pd with elements such as Sn,[26,27] Co,[28] Cu[29] or Bi[30] is effective in increasing electrocatalytic activity and CO tolerance, particularly for the EOR.

The formation of C1 products (e.g., CO and HCOOH) on the surface of the catalyst follows a relatively simple process that includes only a few reaction steps[31,32]. In contrast, the mechanism by which carbon dioxide is reduced to higher-order C2 carbon products is a complex process, and many possible pathways involving electrochemical and chemical steps remain the subject of important theoretical research and debate.[33,34] Different carbon chain growth pathways have been proposed, including electron-mediated dimerization of two adsorbed CO molecules, formation of hydroxy-methyl alkyne intermediates and subsequent non-electrochemical dimerization. Marc Koper et. al provide two pathways for the formation of ethylene in CO reduction on single-crystal copper electrodes. One pathway has a common intermediate with the formation of methane and the other pathway involves selective reduction of CO to ethylene at relatively low overpotentials.[35] They suggest that CO is selectively reduced to C_2H_4 at relatively low overpotentials, presumably through the formation of a surface-adsorbed CO dimer. Here, We discuss the mechanism of hydrogenation of CO_2 by $Pd_{10}Sn_5$ and $Pd_{10}Ag_5$ in detail, and compare the energy under different conditions of gas phase liquid phase. At the same time, the kinetic model is used to calculate the rate constant of each element reaction. Learn the best path to consider the overall response.

2. Computational Method and Details

Density functional theory calculations were performed using the Gaussian 09 packages within the generalized gradient approximation(GGA-PBE).[36] A genecp basis set with a 6-31G(d,p) for C, H atoms and the Los Alamos relativistic effective core potential (RECP) plus DZ basis set (LANL2DZ) for Pd and Cu atoms was employed.[37] The adsorption energies (E_{ads}) were calculated

according to Eq. (6),

$$E_{ads} = E_{total} - E_{substrate} - E_{adsorbate} \tag{6}$$

To determine the thermochemical reaction energetics for CO_2RR along different pathways, the standard equilibrium potentials of electrochemical steps were computed using the computational hydrogen electrode (CHE) model.[38, 39] At $U=0V$ versus RHE, protons and electrons are at equilibrium with H_2 at 101325 Pa, 298 K, and all pH values:
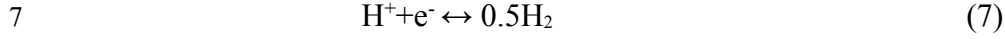
$$H^+ + e^- \leftrightarrow 0.5H_2 \tag{7}$$

Thermodynamics shows that the free energy in the equilibrium reaction changes to zero, so the chemical potential (μ) ：

$$\mu[H^+ + e^-] = 0.5\mu[H_2] - eU \tag{8}$$

The limiting potential U_L is the least negative potential to make the reaction path thermodynamically exergonic (downhill), thus U is an important index to represent the performance of a catalyst. For reaction:

$$A^* + H^+ + e^- \rightarrow AH^* \tag{9}$$

The free energy change of the elementary reaction is:

$$\Delta G = \mu[AH^*] - \mu[A^*] - \mu[H^+ + e^-]$$
$$= \mu[AH^*] - \mu[A^*] - 0.5\mu[H_2] + eU \tag{10}$$

when $U = U_L$, $\Delta G = 0$, so the U_L is:

$$U_L = -\mu[AH^*] - \mu[A^*] - 0.5\mu[H_2] \, (U = 0)/e$$
$$= -\Delta G \text{ V/e} \tag{11}$$

The free energy of each species were calculated by the following formulas:

$$G = H - TS \tag{12}$$

at temperatures greater than 0 K and constant pressure, enthalpy for a given temperature (here $T = 298.15$ K) can be expressed in terms of H_0 and the heat capacity, C_P:

$$H = H + \int C_p \, dT \tag{13}$$

in addition, the entropy term can be expressed as the sum of the translational, rotational, vibrational, and electronic contributions as to:

$$S = S_t + S_r + S_v + S_e \tag{14}$$

and also, intrinsic zero point energy (ZPE) and extrinsic dispersion (D) corrections can be included to finally obtain:

$$G = H + \int C_p dT - T(S_t + S_r + S_v + S_e) + ZPE + D \tag{15}$$

$$\Delta G = \Delta H + \Delta \int C_p dT - T\Delta(S_t + S_r + S_v + S_e) + \Delta ZPE + \Delta D \tag{16}$$

1   For equation (16), we choose to apply some approximations. First, S_e is approximately zero

2   at the fundamental electronic level, and secondly, for the gas, translation, rotation, and vibration

3   entropy terms, there may be a contribution that may not be ignored, therefore: $S = S_t + S_r + S_v$, but

4   for solids and adsorbates, $S_t \approx 0$ and $S_r \approx 0$, therefore: $S = S_v$. Finally, since $\int C_P dT$ is almost

5   negligible and $\int C_P dT \approx 0$, no thermal corrections for the enthalpy have been taken into account

6   for the G calculation. The free energy of each species can calculated by the following formulas:

7    $$G = E_{elec} + ZPE - TS \qquad (17)$$

8   G is the free energy, E_{elec} is the electronic energy of the species from the DFT calculation,

9   ZPE is the zero-point energy, T is the temperature and S the entropy. Those can be obtained using

10   the calculated vibrational frequencies.In accordance with Peterson et al,[40] we do know the free

11   energy difference between two adjacent intermediates $G(U)$ is expressed as a linear function of

12   applied bias potential U:

13    $$G(U) = G_{(U=0)} + neU \qquad (18)$$

14   Where n is the number of the proton-electron pairs transferred to CO_2 and e is the positive

15   elementary charge. The rate-limiting step is the one with the maximum $G(U)$.

16   ## 3. Results and Discussion

17   ## 3.1. Mechanism of C1 Formation on $Pd_{10}Sn_5$ and $Pd_{10}Ag_5$ in the

18   ## Gas-Phase Model.

19   Figure 1 shows the calculated Gibbs free energy (ΔG) diagrams for reducing CO_2 to C1

20   through different reaction steps. The asterisk (*) indicates the surface catalytic active site. As

21   shown in Figure 1, the C1 products involved are CO, HCOOH, CH_4, CH_3OH. The type of reaction

22   is more complicated. Since CO is a valuable product widely used in the chemical industry, and

23   COOH is a key intermediate for CO_2 to form CO, it is essential for its research. Activation of CO_2

24   by formation of HCOO* intermediates is also a common method compared to the formation of

COOH* intermediates to activate CO_2, although both show an uphill energy barrier for the first proton-coupled electron transfer step. Obviously, the ΔG required to form HCOO is lower compared to COOH, indicating a lower onset potential requirement for the CO_2RR of the Pd-Sn surface. The specific combination configuration shown in Figure 2, it shows that the lower or higher origin of ΔG for each step involved in the CO_2 reduction on $Pd_{10}Sn_5$. For example, the structure can explain why HCOO has a lower energy of reaction than COOH. It is noticeable that, when HCOO is formed on the surface of $Pd_{10}Sn_5$, one O in HCOO binds to Pd, and the other O combines with Sn, and a double bond is formed between C and O. This binding configuration will enhance the stability of the adsorbed HCOO compared to the COOH formed on the surface of $Pd_{10}Sn_5$ only bound by C and Pd. The stability of HCOO makes the unique product of HCOOH formation very difficult (endothermic), but its formation has become easier (exothermic) by COOH. The subsequent step of producing adsorbed CO is faster than the free energy of HCOOH. It shows that the stability of CO is greater than HCOOH, this is consistent with the conclusion that the adsorption of CO* is relatively strong on Cu, Pd and Pt.[41]

However, the subsequent hydrogenation steps are extremely difficult, regardless of HCOOH or CO. The reaction pathway of HCOOH is more complicated than CO. For HCOOH, it may formats the C-H bond or the fracture of C-O bond, that is HCOOH→H_2COOH or HCOOH→HCO+OH. Structurally, the cleavage of the C-O bond is easier to occur than the formation of the C-H bond due to the steric effect. Their Gibbs free energy differs by 0.28 eV.

The formation of the C-H bond is the next process by which the CO proceeds. (Although COH can be formed by the O-H bond to form the intermediate C, the energy required for these two steps is no longer suitable for the study of the mechanism, indicated by a red line in Figure 1).

Interestingly, the production of CHO is the common choice of both, but from the energy point of view, the hydrogenation of CO is not easy (ΔG=0.82 eV). This is followed that a CHO* intermediate followed by protonation to form CH_2O* and CH_3O*. The alternating path is the hydrogenation of the CHO* intermediate to form an O-H bond, the formation of the CHOH intermediate as the presence of the CH_2OH intermediate, and of course the opportunity for the appearance of CH_X. Whether CH_3O* or CH_2OH, they end up in only one direction, which is the product of CH_3OH. Once CHOH* is formed, it will go through a series of hydrogenation steps to form the CHx* species and finally produce CH_4. But from the energy point of view, the formation

1   of CHOH is not so easy. The change of 1.20 eV in Gibbs free energy provides evidence that CH_4

2   production is kinetically prohibited and CH_3OH is the preferred C1 product of the reduction path

3   via the CHO* intermediate on $Pd_{10}Sn_5$. The structure of each intermediate is listed in Figure 2.

4   There is nothing special about the bonding. It is worth noting that during this series of reactions,

5   the independent OH groups formed will be further hydrogenated to form a stable water molecule.

6   This is in agreement with experimental reports of CH_2O* reduction on Cu (111) electrodes

7   predominantly producing methanol. The activation of CO_2 through the formation of a COOH*

8   intermediate is the potential-determining step (PDS) for all three facets. According to the above

9   description, Figure 2 shows the structure diagram of CO_2 during the electroreduction of $Pd_{10}Sn_5$ to

10   C1. The left side shows the formation process of CH_4, and the right side shows the formation

11   process of CH_3OH. The biggest difference between the two is the bonding of the left part. The

12   way is through the interaction of C atoms with the catalyst, while the O atom on the right also

13   participates in the bonding. Even in CH_3O, C and the catalyst do not participate in the bonding,

14   and the O atom becomes a bridge between the catalyst and the intermediate. Similarly, the reaction

15   process in which CO_2 is reduced to C1 on $Pd_{10}Ag_5$ has also been studied. The mechanism diagram

16   is given in Figure 1, and the structure diagram is given in Figure 3.

17   For the structure, all intermediates in the formation of C1 products prefer to bind to Pd sites

18   on Pd/Ag, and the adsorption configuration is the same as on Pd/Sn. The minimum-energy

19   pathway of CO_2 electroreduction to C1 at 0 V vs reversible hydrogen electrode (RHE) on $Pd_{10}Ag_5$

20   in the gas-phase model is shown in Figure 1-(2). As with $Pd_{10}Sn_5$, the initial hydrogenation step is

21   to add a proton-electron pair to CO_2*, resulting in the formation of COOH*, which is adsorbed on

22   the surface by carbon binding to the Pd atoms. Similarly, the competitive reaction of this

23   proton-electron transfer process is the formation of HCOO*, which is adsorbed on the surface by

24   the two oxygen-bonded two oxygens bonded to adjacent Pd and Ag atoms, respectively. The

25   reaction energies (Er) of these two steps were E_r = 0.41 eV and E_r = 0.16 eV, respectively.

26   Obviously, the formation of HCOO is extremely advantageous, and this result is easier than 0.22

27   eV on $Pd_{10}Sn_5$. This is given by the fact that HCOO is bonded to the two bonds. The bond length

28   of oxygen and two metals formed on $Pd_{10}Sn_5$ is 2.29 Å and 2.16 Å, respectively. The bond lengths

29   of oxygen and the two metals on $Pd_{10}Ag_5$ were 2.29 Å and 2.09 Å, respectively. The next

30   hydrogenation process of COOH* results in the formation of CO* with Er = −0.55 eV. The

1   alternative formation of HCOOH* in this protonation process is endothermic with 0.53 eV,

2   suggesting that the reduction of COOH* to CO* is more favorable thermodynamically. As in the

3   case of $Pd_{10}Sn_5$, the COOH does not appear in the optimum mechanism because the hydrogenation

4   of CO to CHO is accompanied by $E_r = 0.71$ eV, and there is no advantage compared with the fact

5   that the CO bond in HCOOH is broken to form CHO $E_r = -0.11$ eV.

6   The next hydrogenation process of CHO* results in the formation of CH_2O* with $E_r = 0.33$

7   eV. The alternative formation of CHOH* in this protonation process is endothermic with 1.11 eV,

8   suggesting that the reduction of CHO* to CH_2O* is more favorable thermodynamically. CH_2O * is

9   further hydrogenated to CH_3O *, $E_r = 0.28$ V, wherein CH_3O* is adsorbed onto the catalyst by

10   oxygen, and the methyl group is away from the surface.

11   Whereas the alternative hydrogenation to form CH_2OH* is also endothermic by 0.15 eV, the

12   reaction energy of CH_2O* to CH_2OH* is much more exothermic than that of CH_2O* to CH_3O*.

13   Accordingly, the protonation step of CH_2O* to CH_2OH* is more favorable thermodynamically.

14   Further hydrogenation to CH_2OH* is a key point that determines the formation of CH_3OH by

15   adding the hydrogen to oxygen, or the formation of CH_4 by breaking the C−O bond (followed by a

16   hydrogenation step). It can be seen from the mechanism diagram that the optimal catalytic

17   mechanism for the electrochemical reduction of CO_2 by $Pd_{10}Sn_5$ and $Pd_{10}Ag_5$ is the same, and CH_4

18   is more stable than CH_3OH on the catalyst surface, but the formation process of CH_3OH is easier.

19   It is concluded that in the gas phase model, the best product for the electroreduction of CO_2 to C1

20   is CH_3OH, which is consistent with the experimental results of electroreduction of CO_2 on the

21   surface of $Cu_2O(100)$[42,43] and the best mechanism is $CO_2 \rightarrow HCOO \rightarrow HCOOH \rightarrow CHO \rightarrow$

22      $CH_2O \rightarrow CH_2OH \rightarrow CH_3OH$.

3.2. Mechanism of C1 Formation on $Pd_{10}Sn_5$ and $Pd_{10}Ag_5$ in the

Solvation Model.

25   The role of CO_2 reduction to various hydrocarbon products has been widely recognized, and

26   the influence of the reaction environment on this mechanism has also become the focus of

27   research. Here, a PCM model is introduced to explore the role of solvation. A series of possible

28   CH_3OH and CH_4 reaction pathways and corresponding energetics have been calculated to

29   understand the electroreduction selectivity and efficiency of CO_2 on $Pd_{10}Sn_5$ and $Pd_{10}Ag_5$. Figure

1-(3) shows the minimum energy pathway for CH_3OH on $Pd_{10}Sn_5$ in a solvation model. Under solvation conditions, the electroreduction of CO_2 to CH_3OH exhibits a different reaction pathway. For the first protonation of CO_2^*, there are still two bonding modes, and the formation of HCOO is more favorable than the high energy of COOH formation ($E_r = 0.43$ eV) by forming an O-H bond, and $E_r = 0.15$ eV. In contrast to the reactivity of the two in the gas phase model, it is clear that the effect of solvation alters the reaction energy of the intermediate and thermodynamically accelerates the formation of HCOO*. However, it has caused difficulty in the formation of HCOOH, which can be generated only in the gas phase by 0.35 eV, and 0.44 eV in the liquid phase model.

The third protonation step leads to the formation of CHO*, where the reaction in the liquid phase is slightly promoted to less than 0.01 eV, and the position of the rapid step does not change as the reaction environment changes. The alternative protonation process of CHO* to CHOH* is also significantly refrained in the solvation condition ($E_r = 1.24$ eV). And its competition step CHO* to CH_2O is significantly promoted, making the hydrogenation process of CHO simple. The difficulty in forming CHOH makes the formation of CH_X more difficult. The reaction mechanism is changed in the further protonation of CH_2O *, and the formation of the stable intermediate CH_2OH in the gas phase is not dominant in the liquid phase, so that the formation of CH_3O becomes the main body, and then CH_3OH is formed. It clearly shows that the liquid phase not only changes the adsorption performance of the intermediate, but also participates in the CO_2 electroreduction process. And solvation alters the protonation of the intermediate on the surface of $Pd_{10}Sn_5$ and results in the formation of CH_3OH without CH_4, which further suggests that the effect of solvation is critical for CO_2 electroreduction. Solvation affects different catalysts, as well as for electrochemical reduction of CO_2. It can be concluded that the reaction mechanism of electrochemical reduction of CO_2 in $Pd_{10}Sn_5$ is CO_2 → HCOO → HCOOH → CHO → CH_2O → CH_3O → CH_3OH. $Pd_{10}Sn_5$ has little effect on solvation. Although the mechanism changes slightly, it has little change compared with $Pd_{10}Ag_5$.

On $Pd_{10}Ag_5$ under the influence of solvation, the only constant remain is the individual intermediates involved in the best mechanism. However, only the type of the intermediate did not change, and the change in energy made the electrochemical reduction reaction of CO_2 on $Pd_{10}Ag_5$ extremely disadvantageous. The mechanism of its optimal path is proposed in the gas phase. The

The first step is the hydrogenation of CO_2 to form HCOO, which requires an increase of 0.06 eV compared to the gas phase model. The second step reaction is the rate-determining step of this mechanism. The process in the gas phase model is not very difficult (Er = 0.53 eV), while the reaction energy in the liquid phase becomes 0.87 eV. Further, the formation of the CH_3OH is an exothermic reaction in the gas phase, and this step changes an endothermic reaction in the liquid phase. It indicates that the synergic effect of the atomic structure of catalysts and the solvation plays a crucial role in determining the selectivity of product.

3.3 Mechanism of C2 Formation on $Pd_{10}Sn_5$ and $Pd_{10}Ag_5$ in the Gas-Phase Model.

Structurally, the formation of the C1 product is mainly due to the bonding of the C atom in the intermediate to the Pd atom on the catalyst. Regardless of whether it is $Pd_{10}Ag_5$ or $Pd_{10}Sn_5$, the Pd atom is the active center. In this way, we further explore the possibility of the C2 approach. Compared to the C1 product, the C2 pathway is more complex and involves a large number of intermediates. Here, the structural diagrams of the intermediates in which CO_2 to CH_3CH_2OH are shown in Figures 4 and 5, respectively. The adsorption configuration of the intermediates is similar despite the different catalysts, which is why the Pd atoms are active centers. As with most studies, the formation of C-C bonds is formed by the dimerization of CO. The formation of CO has been described in the previous section, which involves the transfer of two pairs of proton electron pairs. This figure is divided into nine rows, each of which involves a process of proton electron pair specificity, each process involving a different number of intermediates, and the structure of each intermediate will be described in turn.

The structure of the first row of COCO is formed by CO dimerization. Two C atoms are bonded to the same Pd atom. The bond length is 2.05 Å and 2.08 Å, respectively. The bond lengths in $Pd_{10}Ag_5$ are 1.98Å and 1.99Å, respectively. Although this structure involves two C-O double bonds, this step is not so stable that it cannot be detected in the experiment, so its hydrogenation should be extremely rapid, and it is responsible for the C-C bond breaking and causing CO accumulation. The C-C bond length of CO-COH is 1.46 Å, which is different from the

1   values of 1.29 Å and 1.33 Å found in the gas phase by C_2O_2 and C_2H_4, indicating the presence of a

2   single C-C bond.

3   The second line involves two intermediates, one is the COCOH formed by forming an O-H

4   bond, and the step of competing is to form a C-H bond to form CHOCO. The two are very

5   different in energy. The stability of CHOCO is much larger than that of COCOH, mainly because

6   in CHOCO, not only the C atom and the catalyst act, but also the O atom and the Ag and Sn atoms

7   bond, which increases its stability. At the beginning of the third row, the graphics became very

8   complicated, involving four intermediates: CCO, CHOCHO, CHOHCO, CH_2OCO. The

9   adsorption configuration of the four intermediates are different, in which the three structures CCO,

10   CHOHCO, and CH_2OCO are perpendicular to the catalyst, and CHOCHO is parallel to the

11   catalyst, which increases the contact area with the catalyst. Its stability increases. The most

12   difficult of these four intermediates is CH_2OCO, because one of its C atoms bonds with C, O and

13   two H atoms, causing the C atom to become saturated and unable to interact with the catalyst.

14   Lack of bonding with the catalyst, so its stability is the worst.

15   The fourth line involves six intermediates, C-CHO, HCCO, CH_2OCHO, CH_2OHCO,

16   CHOHCHO, CCOH. The bonding types of these six intermediates can be divided into four types,

17   in which both CCHO and CCOH are bonded to Pd and the other atoms do not interact with the

18   catalyst. The bonding mode of CH_2OCHO and CH_2OHCO is more complicated than that. On the

19   basis of C, O also participates in the bonding, which increases the effect of the catalyst. In HCCO,

20   two C atoms are bonded to different Pd atoms on the catalyst. On the atom. The last type of

21   bonding is the most complicated. It includes all the above bonding methods, what are, two C

22   atoms and O atoms participate in the bonding, and the whole is parallel to the catalyst surface,

23   which increases the contact area. The most stable intermediate you need to find.

24   The fifth line involves six intermediates, HCCHO, CH_2CO, CH_2OHCHO, $CHOHCH_2O$,

25   HCC-OH, C-CHOH, C-CH_2O. As the number of atoms increases, the bonding of C atoms is close

26   to saturation, so most of the intermediates involved in this step are a C atom and an O atom

27   participating in the bonding. Among these intermediates, for HCCHO, the addition of bonds

28   between a C atom and two atoms, together with the addition of an O atom, makes it the most

29   stable intermediate in this step. The sixth line involves five intermediates, CH_2CHO, CH_3CO,

30   HCCHOH, $HCCH_2O$, H_2CCOH. The stability of these five intermediates is quickly answered by

their way of bonding. First of all, each intermediate involves a double bond, or a C-C double bond, or a C-O double bond. In addition to $HCCH_2O$, there is one of the most unstable intermediates. Among the remaining four, three are C and O bonded to the catalyst, except that CH_2CHO remains parallel to the catalyst, the most stable intermediate is it. The seventh line involves five intermediates, CH_3CHO, CH_2CHOH, CH_3COH, CH_2CH_2O, $CHCH_2OH$. The most stable intermediate is CH_3CHO, which has two C atoms bonded to each other in the molecule to form a bond, and a bond between the O atom and the Pd atom. The eighth line involves three intermediates, CH_3CHOH, CH_2CH_2OH, CH_3CH_2O. The most stable intermediate is CH_3CHOH. This is followed by the formation of the CH_3CH_2OH.

It has previously been determined that CO_2 is converted to CO prior to further reduction; in addition, compounds from CO to C2 are better established and have been extensively studied. [44,45] Therefore, we specialize in the reduction mechanism after CO dimerization. Because this process determines the selectivity of CO_2RR, previous studies have taken a similar approach.

Calle-Vallejo and Koper[46] proposed CO dimerization as the first step toward C2 products. C-C bond lengths are useful to track the presence of multiple bonds in the intermediates. Cheng et al.[47] built upon this idea to devise a more complete mechanism in which CO dimerization is followed by hydrogenation of an oxygen atom (*COCO + H → *COCOH). However, according to the energies provided in our calculation, *COCHO, precursor of for example, glyoxal, is less stable than *COCOH by 1.09 eV on $Pd_{10}Sn_5$ and 1.07 eV on $Pd_{10}Ag_5$, suggesting a more favorable initial hydrogenation of the C atoms in C_2O_2. And the difference between the two is so obvious, indicating that the COCHO is the key intermediate in the conversion of CO_2 to C2 compounds on $Pd_{10}Sn_5$ or $Pd_{10}Ag_5$, and there is no advantage in the competitive step.

From this point, the subsequent proton–electron additions proceed such that the C-O double bond is preserved: the next step is alpha-carbon protonation (CH_2OCO), or the protonation of the C atom in the carbonyl (*CHOCHO) or O forms a chemical bond before C (CHOHCO or CHOCOH). Structurally, CHOCHO is considered the most stable intermediate, and the reaction energy is also verified. For CHOCO →* CHOCHO, the reaction energy on $Pd_{10}Sn_5$ is -0.13 eV, and other competitive steps are endothermic reactions. The reaction on $Pd_{10}Ag_5$ is an endothermic reaction. Compared with other products, the reaction energy required to form CHOCHO is the least, which is 0.18 eV. The next step is to discuss the protonation of CHOCHO. The symmetry of

1　CHOCHO makes its protonation process simple, either by forming a CH_2OCHO via a C-H bond

2　or by forming a CHOHCHO via an O-H bond. The stable intermediate given in the structure is

3　CHOHCHO, ie the bond of O to hydrogen is preferred over C. This is consistent with the results

4　given by the reaction. For $Pd_{10}Sn_5$, the protonation energy fluctuation of CHOCHO is very mild.

5　Regardless of endotherm (formation of CH_2OCHO) or exotherm (formation of CHOHCHO), the

6　change in energy value is very small, 0.03 eV and -0.07 eV, respectively. On $Pd_{10}Ag_5$, the positive

7　and negative changes of the reaction energy are consistent with the above, but the magnitude of

8　the energy change is large, 0.34 eV and -0.30 eV, respectively. This shows that the next step

9　begins with CHOHCHO. The difference between $Pd_{10}Sn_5$ and $Pd_{10}Ag_5$ is reflected here.

10　　　In the previous discussion, it was proposed that the interaction between CH_2OHCHO and

11　HCCHO and the catalyst is very strong, and both of them can be formed by the protonation of

12　CHOHCHO. The value of the reaction energy becomes the sole criterion for judging the stability

13　of the two. On $Pd_{10}Sn_5$, the reaction energy for generating CH_2OHCHO is 0.01eV for the

14　formation of HCCHO at 0.22eV, which is 0.21eV, which indicates that CH_2OHCHO is stable. The

15　reaction energy for generating CH_2OHCHO on $Pd_{10}Ag_5$ is 0.44eV. 0.13 eV, the difference between

16　the two is 0.31 eV, indicating that the stability is HCCHO. Therefore, the mechanism of

17　conversion of CO_2 to the C2 compound on $Pd_{10}Sn_5$ and $Pd_{10}Ag_5$ is not completely consistent.

18　　　With the next step, CH_2CHO was produced, and CH_2CHO was the most stable intermediate

19　in both $Pd_{10}Sn_5$ and $Pd_{10}Ag_5$. The reaction energies is -0.59 eV and -0.12 eV, respectively. The

20　type of intermediates remains the same, first the protonation of α-C forms CH_3CHO, followed by

21　the hydroxylation of the O atom to form CH_3CHOH, which ultimately forms the desired product.

22　The reaction energies of this series of processes on $Pd_{10}Sn_5$ is -0.32 eV, 0.57 eV, -0.61 eV,

23　respectively. It can be seen that the hydroxylation of the O atom is more difficult than the

24　protonation process of α-C, and in this mechanism, the hydroxylation of the O atom of CH_3CHO

25　to form CH_3CHOH is a rate-limiting step to form ethanol. Also on the $Pd_{10}Ag_5$ series reaction

26　energies of the process is -0.43 eV, 0.25 eV, -0.25 eV, respectively. The rate-limiting step is still

27　the hydroxylation of the O atom of CH_3CHO. Summarize the above is, the minimum-energy

28　pathway of CO_2 electroreduction to CH_3CH_2OH at 0 V vs reversible hydrogen electrode (RHE) on

29　$Pd_{10}Sn_5$ and $Pd_{10}Ag_5$ in the gas-phase model is:COCO* → CHOCO* → CHOCHO*

30　→CHOHCHO* → CH_2OHCHO* (CHCHO)→ CH_2CHO→CH_3CHO* → CH_3CHOH* →

CH$_3$CH$_2$OH. The most favorable pathway for CO$_2$RR catalyzed by Pd$_{10}$Sn$_5$ is shown in Figure 4. Analyzing the potential energy surface, we found that the most uphill step (the potential-determining step) is the reduction: *CH$_3$CHO → CH$_3$CHOH with ΔG = 0.57 eV. This means at −0.57 VRHE, the free-energy change for each step is either zero or downhill. For Pd$_{10}$Ag$_5$,the value is 0.25eV.

3.4 Mechanism of C2 Formation on on Pd$_{10}$Sn$_5$ and Pd$_{10}$Ag$_5$ in the Solvation Model.

For all the intermediate in the gas phase, we also calculated all in the liquid phase. Considering electrochemical reduction of COCO in Pd$_{10}$Sn$_5$, from the Figure 4, we find that the protonation of CH$_3$CHO has changed dramatically in the liquid environment. The data illustrates the changes. The protonation of CH$_3$CHO is controversial here: whether the C atom is protonated or the O atom is protonated first. The reaction energies for the formation of CH$_3$CHOH and CH$_3$CH$_2$O in a gas phase is 0.57 eV and 0.84 eV, respectively, so that the O atom is preferentially protonated. The reaction energies of CH$_3$CHOH and CH$_3$CH$_2$O in the liquid phase are 0.44 eV and 0.20 eV, respectively, and the C atoms are preferentially protonated. Therefore, the liquid reaction has a stabilizing effect on the intermediate CH$_3$CH$_2$O. At Pd$_{10}$Ag$_5$, the stability of the HCCHO intermediate stabilized in the gas phase is reduced in the liquid phase and is replaced by the more stable CH$_2$OHCHO. Figure 7 shows the variation in the U$_L$ for the CO$_2$ reduction that is explicitly calculated for all close-packed surfaces with and without explicit solvation. A less negative U$_L$ corresponds to a smaller theoretical overpotential for reduction. The formation of C2 in Pd$_{10}$Sn$_5$ and Pd$_{10}$Ag$_5$ have a lower U$_L$, suggesting they would be selective towards CH$_3$CH$_2$OH formation if C–C bond formation is viable on these metals. This is also based on experiments. Previous studies by M. T. M. Koper et al. have reported C2 products are formed at low overpotentials without the formation of C1 products on Cu(100)[48].

The type of catalyst and the reaction environment have an effect on the reaction mechanism, which in turn affects the steps of reaction corresponding to the U$_L$ value. Ag-C2 has the same reaction mechanism in the gas phase and liquid phase, and the U$_L$ is for CH$_3$CHO* → CH$_3$CHOH* reduction. The difference between the two is small, indicating that the reaction environment has little effect on the stability of the C-C compound on Pd$_{10}$Ag$_5$. According to the

above description, the reaction mechanism of $Pd_{10}Sn_5$ and $Pd_{10}Ag_5$ for electroreduction of CO_2 to

2 CH_3CH_2OH in liquid phase is COCO* → CHOCO* → CHOCHO* →CHOHCHO* →

3 CH_2OHCHO* → CH_2CHO→CH_3CHO* → CH_3CH_2O*(CH_3CHOH*) → CH_3CH_2OH. However,

4 for the same catalyst, the difference of the U_L between the gas phase and the liquid phase of

5 Ag-C1 is large, and U_L is used for HCOO*→HCOOH* reduction in the gas phase. HCOOH liquid

6 phase greatly affected, it is difficult to carry out hydrogenation HCOO. The direct result is that the

7 process of U_L becomes CO* → CHO*, and CO hydrogenation to CHO has proved to be a difficult

8 step in many studies, so the change in U_L value is obvious. For the $Pd_{10}Ag_5$ catalyst, the liquid

9 phase is extremely detrimental to the formation of the C1 product. The process of the same

10 reaction takes place on the $Pd_{10}Sn_5$ catalyst, and the reaction steps represent the U_L values are

11 HCOOH* → CHO*, both in the gas phase and in the liquid phase. And as the environment of the

12 reaction changes, the value of the U_L remains almost unchanged. However, the difference in the

13 U_L of 0.37 eV in the gas phase and the liquid phase of Sn-C2 makes doubt about the stable

14 intermediates in the formation of C2. It has been calculated that the liquid phase greatly

15 contributes to the stability of CH_3CH_2O, making the reduction reaction involved in the C-C bond

16 extremely easy. This means that as long as CO is formed on $Pd_{10}Sn_5$, the C2 product is easily

17 produced, and the C1 product has almost no competition, and of course it needs to be in a liquid

18 phase. Therefore, a suitable environment of reaction tends to increase the selectivity of the product

19 and avoid the formation of other substances.

20 **3.5 Micro-kinetic modeling**

21 Defining the rate constant of each elementary reaction (k) by the following equation (1),

$$k_i = A'\, exp\left(-\frac{\beta e\left(U - U_i^0\right)}{k_B T} \right)$$

$$A' = \frac{k_B T}{h}\, exp\left(-\frac{\Delta G_i\left(U_i^0\right)}{k_B T} \right)$$

26 where $\Delta G_i(U_i^0)$ is the activation free energy at the reversible potential U_i^0 of step i, and β is a

27 symmetry factor, which, for simplicity, we set to be 0.5. h is the Planck constant and T stands for

28 temperature which was 298.15 K in this study. Despite the difference in the phase conditions, the

29 calculated favorable sites for each adsorbed intermediate species in the considered mechanism

1 under liquid phase conditions were found to be the same as those in the gaseous-phase, resulting

2 in similar structures and relative energies. However, the magnitude of the calculated rate constant

3 will clearly show the structural differences. Therefore, in some cases, introducing the liquid

4 solvent resulted in significant deviations in energies compared to those under gaseous-phase

5 conditions.

6   Taking the reduction of CO_2 to CH_3OH on $Pd_{10}Sn_5$ as an example, Figure 1 shows that the

7 reaction environment has little effect on the optimal mechanism, and the rate constant of each step

8 can be calculated. The results show that only the order of the rate constants in the HCOOH

9 formation and reduction steps is consistent, and the magnitude of the remaining processes varies.

10 Especially for the protonation process of HCOO, the rate constant in the gas phase is 7.23×10^4 s^{-1},

11 while the value in the liquid phase is only 1.4 s^{-1}. It is also an exothermic reaction in

12 thermodynamics, which is a relatively easy process, and the difference between the two can be

13 seen in terms of kinetics. The formation of CH_3OH is an exothermic reaction. The values of the

14 reaction energies of the gas phase and the liquid phase are -0.62eV and -0.3eV, respectively. The

15 corresponding rate constants are 1.24×10^{10} s^{-1} and 2.46×10^7 s^{-1}, respectively. The way to find the

16 best mechanism from the microkinetics through the rate constant is different from the potential

17 energy surface. The smaller the energy change between various reactions on the potential energy

18 surface, the closer to the optimal mechanism. In the kinetics, the larger the exothermic reaction,

19 the greater the energy difference between the two, the larger the rate constant, the faster the

20 reaction process. From the point of view of the rate constant, the process of reducing CO_2 to

21 CH_3OH on $Pd_{10}Ag_5$ is obvious. In addition to promoting the HCOO $\rightarrow$ HCOOH process in the

22 liquid phase process, the values of all other processes indicate that the reaction is difficult in the

23 liquid phase.

24   Unlike the process of forming CH_3OH, the formation of ethanol is discussed after the start of

25 CO dimerization. In $Pd_{10}Sn_5$, eight rate constants represent the completion of the reaction. In the

26 gas phase, the smallest of the eight rate constants is 2.40×10^{-2} s^{-1}, the corresponding process is

27 $CH_3CHO \rightarrow CH_3CHOH$, indicating that this process is a constant speed step, which is consistent

28 with the results in the potential energy surface discussion. The maximum value of 2.02×10^8 s^{-1}

29 corresponds to the formation of the product, namely $CH_3CHOH \rightarrow CH_3CH_2OH$. In the liquid

30 phase, the value of the seventh rate constant is also the smallest, being 5.39×10^7 s^{-1}, but the

corresponding process becomes $CH_3CHO \rightarrow CH_3CH_2O$. Although they are all minimum values, their values are 9 orders of magnitude larger than those in the gas phase, even smaller than the maximum value in the gas phase. Compared with other groups of data, the value of the rate constant in the liquid phase is large. Moreover, the reaction process corresponding to the maximum rate constant is no longer the same as in the liquid phase, and becomes $CH_2OHCHO \rightarrow CH_2CHO$. The above indicates that the liquid phase environment has a stabilizing effect on each intermediate of the C-C substance, and has a good promoting effect on their protonation process, and can reduce the overall reaction energy and shorten the reaction time by changing the reaction environment.

In $Pd_{10}Ag_5$, the liquid phase environment still does not play a positive role in the reaction. In the gas phase, the slowest elementary step is $CH_3CHO \rightarrow CH_3CHOH$, and the rate constant is 3.9×10^6 s^{-1}, which is faster than the fastest step in methanol production, and is also superior to $Pd_{10}Sn_5$. Comparing the reaction rate constants of each step, it can be concluded that the reaction rate constants on $Pd_{10}Ag_5$ are 10^8, 10^3, 10^9, 10^4 faster than those on $Pd_{10}Sn_5$ in the eight processes from COCO to ethanol. $10, 10^7, 10^8, 10^2$ times, although there is a disagreement in the next product of CHOHCHO, it has no effect on its overall. It is indicated that in the gas phase environment, the selectivity of ethanol on the surface of $Pd_{10}Ag_5$ catalyst is greater than that of methanol, and the reaction rate is better than that of another catalyst----$Pd_{10}Sn_5$. As the reaction environment becomes a liquid phase, the situation is completely opposite. For the protonation of the reaction rate step CH_3CHO, the value of the reaction rate constant in $Pd_{10}Sn_5$ is two orders of magnitude larger than that on $Pd_{10}Ag_5$. The advantage of the rate constant of $Pd_{10}Ag_5$ in other processes is no longer, indicating that the liquid reaction environment has different effects on the two catalysts $Pd_{10}Sn_5$ and $Pd_{10}Ag_5$. One is to promote the reaction and improve the stability of the intermediate, and with the participation of Ag. There is no identical result. This indicates that the catalyst $Pd_{10}X_5$ acts not only on the Pd atoms of the active sites but also on the other intermediates such as Sn and Ag atoms. The addition of Sn and Ag atoms changes the environment around the Pd atom in $Pd_{10}X_5$. As the external environment changes, the influence of the added atoms on the cluster is gradually revealed. This combines the structure of the catalyst and the reaction environment. A theoretical reference is provided to design an efficient catalyst together.

4. Conclusion

In this work, we have studied two potential catalysts for the production of hydrocarbons by hydrogenation of carbon dioxide. For the two different bimetallic catalysts of $Pd_{10}Sn_5$ and $Pd_{10}Ag_5$, a KMC simulation based on the first principle was performed. The resulting product C1 was compared to C2. We used DFT calculations to find the most stable alignment of each catalytic surface, simulating the catalytic performance of $Pd_{10}Sn_5$ and $Pd_{10}Ag_5$ in different reaction environments. A complex network of basic reaction steps is assumed. We have shown that in the catalysts studied, the formation of ethanol shows the highest selectivity. On $Pd_{10}Ag_5$, the formation of ethanol is almost unaffected by the environment, and its value of the limit potential is small regardless of the gas phase or liquid phase model. On the $Pd_{10}Sn_5$, the liquid phase environment is more conducive to the production of ethanol. The other two catalysts are less suitable for the production of C1 compounds such as methanol and methane, which gives the same conclusion on the value of the rate constant. This study provides a new avenue to design a electrocatalyst for obtaining a desired CO_2 reduction product.

Notes

[#]Yu Han and Zhijia Zhang are co-first authors.

Conflict of interest

The authors declare that they have no conflict of interest.

1   **References**

2   [1] F.w. Li, L. Chen, M. Xue, T. Williams, Y. Zhang, D.R. MacFarlane, J. Zhang, Towards a better

3   Sn: efficient electrocatalytic reduction of CO_2 to formate by Sn/SnS_2 derived from SnS_2

4   Nanosheets, Nano Energy. 31 (2016) 270-277.

5   [2] V. Scott, S. Gilfillan, N. Markusson, H. Chalmers, R.S. Haszeldine, Last chance for carbon

6   capture and storage, Nat. Clim. Change. 3 (2012) 105-111.

7   [3] B. Kumar, J.P. Brian, V. Atla, S. Kumari, K.A. Bertram, R.T. White, J.M. Spurgeon,

8   Controlling the product syngas $H_2:CO$ ratio through pulsed-bias electrochemical reduction of CO_2

9   on copper, ACS Catalysis. 6 (2016) 4739−4745.

10   [4] S. Guo, S. Zhao, X. Wu, H. Li, Y. Zhou, C. Zhu, N. Yang, X. Jiang, J. Gao, L. Bai, Y. Liu, Y.

11   Lifshitz, A Co_3O_4 -CDots-C_3N_4 three component electrocatalyst design concept for efficient and

12   tunable CO_2 reduction to syngas, Nat. Commun. 9 (2018) 648.

13   [5] H. Xie, T. Wang, J. Liang, Q.Li, S. Sun, Cu-based nanocatalysts for electrochemical reduction

14   of CO_2, Nano Today. 21 (2018) 41−54.

15   [6] G. Zhao, X. Huang, X. Wang, X. Wang, Progress in catalyst exploration for heterogeneous

16   CO_2 reduction and utilization: a critical review, J. Mater. Chem. A. 5 (2017) 21625−21649.

17   [7] Q. Lu, F. Jiao, Electrochemical CO_2 reduction: electrocatalyst, reaction mechanism, and

18   process engineering, Nano Energy. 29 (2016) 439−456.

19   [8] W. Sheng, S. Kattel, S. Yao, B. Yan, Z. Liang, C.J. Hawxhurst, Q. Wu, J.G. Chen,

20   Electrochemical reduction of CO_2 to synthesis gas with controlled CO/H_2 ratios, Energy Environ.

21   Sci. 10 (2017) 1180−1185.

22   [9] B. Khezri, A.C. Fisher, M. Pumera, CO_2 reduction: the quest for electrocatalytic materials, J.

23   Mater. Chem. A. 5 (2017) 8230−8246.

24   [10] M.B. Ross, C.T. Dinh, Y. Li, D. Kim, P. De Luna, E.H. Sargent, P. Yang, Tunable Cu

25   enrichment enables designer syngas electrosynthesis from CO_2, J. Am. Chem. Soc. 139 (2017)

26   9359−9363.

27   [11] I. Ganesh, Conversion of carbon dioxide into methanol - a potential liquid fuel: fundamental

28   challenges and opportunities (a review), renewable sustainable, Energy Rev. 31 (2014) 221−257.

29   [12] H.R. Jhong, S.C. Ma, P.J.A. Kenis, Electrochemical conversion of CO_2 to useful chemicals:

current status, remaining challenges, and future opportunities, Curr. Opin. Chem. Eng. 2 (2013) 191−199.

[13] C. Oloman, H. Li, Electrochemical processing of carbon dioxide, ChemSusChem 1 (2008) 385−391.

[14] D.T. Whipple, P.J.A. Kenis, Prospects of CO_2 utilization via direct heterogeneous electrochemical reduction, J. Phys. Chem. Lett. 1 (2010) 3451−3458.

[15] Z. Sun, T. Ma, H. Tao, Q. Fan, B. Han, Fundamentals and challenges of electrochemical CO_2 reduction using two-dimensional materials, Chem. 3 (2017) 560−587.

[16] X.Liu, H. Yang, J. He, H. Liu, L. Song, L. Li, J. Luo, Highly active, durable ultrathin $MoTe_2$ layers for the electroreduction of CO_2 to CH_4, Small 14 (2018) 1704049.

[17] K. Jiang, R.B. Sandberg, A.J. Akey, X. Liu, D.C. Bell, J.K. Nørskov, K. Chan, H. Wang, Metal Ion cycling of Cu foil for selective C−C coupling in electrochemical CO_2 reduction, Nat. Catal. 1 (2018) 111−119.

[18] D Kim, J. Resasco, Y. Yu, A.M. Asiri, P. Yang, Synergistic geometric and electronic effects for electrochemical reduction of carbon dioxide using gold-copper bimetallic nanoparticles, Nat. Commun. 5 (2014) 4948.

[19] H.Xie, T. Wang, J. Liang, Q. Li, S. Sun, Cu-based nanocatalysts for electrochemical reduction of CO_2, Nano Today 21 2018 41−54.

[20] W. Zhu, R. Michalsky, Ö. Metin, H. Lv, S. Guo, C.J. Wright, X. Sun, A.A. Peterson, S. Sun, Monodisperse Au nanoparticles for selective electrocatalytic reduction of CO_2 to CO, J. Am. Chem. Soc. 135 (2013) 16833−16836.

[21] G.A.Somorjai, Y. Li, Introduction to surface chemistry and catalysis, Wiley: New York, 2010.

[22] R. Mu, Q. Fu, H. Xu, H. Zhang, Y. Huang, Z. Jiang, S. Zhang, D. Tan, X. Bao, Synergetic effect of surface and subsurface Ni species at Pt-Ni bimetallic catalysts for CO oxidation, J. Am. Chem. Soc. 133 (2011) 1978−1986.

[23] F. Tao, Synthesis, Catalysis, Surface chemistry and structure of bimetallic nanocatalysts, Chem. Soc. Rev. 41 (2012) 7977−7979.

[24] S. Carri´on-Satorre, M. Montiel, R. Escudero-Cid, J.L.G. Fierro, E. Fat´as and P. Oc´on, Performance of carbon-supported palladium and palladiumruthenium catalysts for alkaline membrane direct ethanol fuel cells， Int. J. Hydrogen Energy 41 (2016) 8954-8962.

[25] H. An, L. Pan, H. Cui, B. Li, D. Zhou, J. Zhai and Q. Li, Synthesis and performance of palladium-based catalysts for methanol and ethanol oxidation in alkaline fuel cells ， Electrochimica Acta 102 (2013) 79-87.

[26] A.N. Geraldes, D. Furtunato da Silva, J.C. Martins da Silva, O. Antonio de S´a, E.V. Spinac´e, A.O. Neto, M. Coelho dos Santos, Palladium and palladium–tin supported on multi wall carbon nanotubes or carbon for alkaline direct ethanol fuel cell, J. Power Sources 275 (2015) 189–199.

[27] Z. Luo, M. Ib´a˜nez, A.M. Antol´ın, A. Genç, A. Shavel, S. Contreras, F. Medina, J. Arbiol, A. Cabot, Size and aspect ratio control of Pd_2Sn nanorods and their water denitration properties, Langmuir 31 (2015) 3952–3957.

[28] A.-L. Wang, X.-J. He, X.-F. Lu, H. Xu, Y.-X. Tong, G.-R. Li, Palladium‐Cobalt nanotube arrays supported on carbon fiber cloth as high-performance flexible electrocatalysts for ethanol oxidation, Angew. Chem., Int. Ed., 54 (2015) 3669–3673.

[29] H. Na, L. Zhang, H. Qiu, T. Wu, M. Chen, N. Yang, L. Li, F. Xing , J. Gao, A two step method to synthesize palladium–copper nanoparticles on reduced graphene oxide and their extremely high electrocatalytic activity for the electrooxidation of methanol and ethanol, J. Power Sources 288 (2015) 160–167.

[30] J. Cai, Y. Huang and Y. Guo, Bi-modified Pd/C catalyst via irreversible adsorption and its catalytic activity for ethanol oxidation in alkaline medium, Electrochim. Acta 99 (2013) 22-29.

[31] R. Kortlever, J. Shen, K.J.P. Schouten, F. Calle-Vallejo, M.T.M. Koper, Catalystsand reaction pathways for the electrochemical reduction of carbon dioxide, J. Phys. Chem. Lett. 6 (2015) 4073–4082.

[32] J. Rosen, G.S. Hutchings, Q. Lu, S. Rivera, Y. Zhou, D.G. Vlachos, F. Jiao, Mechanistic insights into the electrochemical reduction of CO_2 to CO on nanostructured Ag surfaces, ACS Catal. 5 (2015) 4293–4299.

[33] R. Kas, R. Kortlever, H. Yılmaz, M.T.M. Koper, G. Mul, Manipulating the hydrocarbon selectivity of copper nanoparticles in CO_2 electroreduction byprocess conditions, ChemElectroChem 2 (2015) 354–358.

1 [34] L. Ou, W. Long, Y. Chen, J. Jin, New reduction mechanism of CO dimer by hydrogenation to

2 C2H4on a Cu(100) surface: theoretical insight into thekinetics of the elementary steps, RSC Adv.

3 5 (2015) 96281−96289.

4 [35] K.J. Schouten, Z. Qin, G.E. Pérez, M.T. Koper, Two pathways for the formation of ethylene

5 in CO reduction on single-crystal copper electrodes, J. Am. Chem. Soc. 134 (2012) 9864−9867.

6 [36] M.J. Frisch, G.W. Trucks, H.B. Schlegel, G.E. Scuseria, M.A. Robb, J.R. Cheeseman, G.

7 Scalmani, V. Barone, B. Mennucci, G.A. Petersson, Gaussian 09, revision A.1, Gaussian,

8 Wallingford, CT, 2009.

9 [37] P. J. Hay, W. R. Wadt, J. Chem. Phys., 1985, 82, 270-283.

10 [38] J.K. Nørskov, J. Rossmeisl, A. Logadottir, L. Lindqvist, J.R. Kitchin, T. Bligaard, H. Jónsson,

11 Origin of the overpotential for oxygen reduction at a fuel-cell cathode, J. Phys. Chem. B 108

12 (2004) 17886−17892.

13 [39] A.A. Peterson, F. Abild-Pedersen, F. Studt, J. Rossmeisl, J.K. Nørskov, How copper

14 catalyzes the electroreduction of carbon dioxide into hydrocarbon fuels, Energ. Environ. Sci. 3

15 (2010) 1311−1315.

16 [40] A.A. Peterson, J.K. NØrskov, Activity descriptors for CO_2 electroreduction to methane on

17 transition-metal catalysts, J Phy Chem Lett, 3 (2012) 251-258.

18 [41] Z. Zhao, G. Lu, Computational screening of near-surface alloys for CO_2 electroreduction,

19 ACS Catalysis (2018) 7b03705.

20 [42] T.Y. Chang, R.M. Liang, P.W. Wu, J.Y. Chen, Y.C. Hsieh, Electrochemical reduction of CO_2

21 by Cu_2O-catalyzed carbon clothes, Mater. Lett. 63 (2009) 1001−1003.

22 [43] M. Le, M. Ren, Z. Zhang, P.T. Sprunger, R.L. Kurtz, J.C. Flake, Electrochemical reduction

23 of CO_2 to CH_3OH at copper oxide surfaces, J. Electrochem. Soc. 158 (2011) E45−E49.

24 [44] T. Cheng, H. Xiao, W.A. Goddard , Reaction mechanisms for the electrochemical

25 reductionof CO_2 to CO and formate on the Cu(100) surface at 298K from quantum mechanics free

26 energy calculations with explicit water, J. Electrochem. Soc. 138 (2016) 13802-13805.

27 [45] W. Luo, X. Nie, M.J. Janik, A. Asthagiri, Facet dependence of CO_2 reduction paths on Cu

28 electrodes, ACS Catal. 6 (2016) 219−229.

29 [46] F. Calle-Vallejo, M.T.M. Koper, Theoretical considerations on the electroreduction of CO to

30 C_2 Species on Cu(100) Electrodes, Angew. Chem., Int. Ed. 52 (2013) 7282−7285.

1   [47] T. Cheng, H. Xiao, W.A. Goddard, Full atomistic reaction mechanism with kinetics for CO

2   reduction on Cu(100) from ab initio molecular dynamics free-energy calculations at 298 K, Proc.

3   Natl. Acad. Sci. U. S. A. 114 (2017) 1795-1800.

4   [48] K.J.P. Schouten, Z. Qin, E.P. Gallent, M.T.M. Koper, Two pathways for the formation of

5   ethylene in CO reduction on single-crystal copper electrodes, J. Am. Chem. Soc. 134 (2012)

6   9864–9867.

7

Scheme 1. Reaction network for CO_2 reduction to C1 compounds
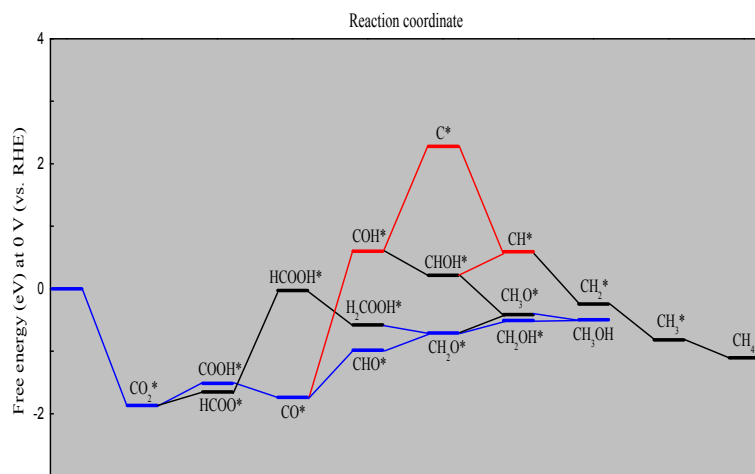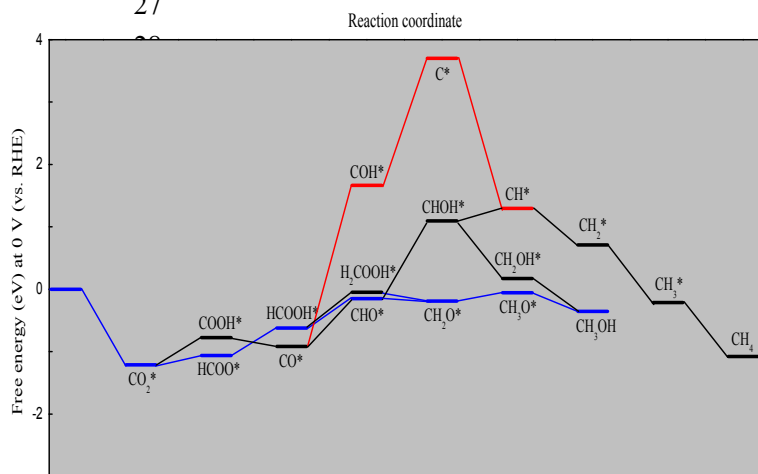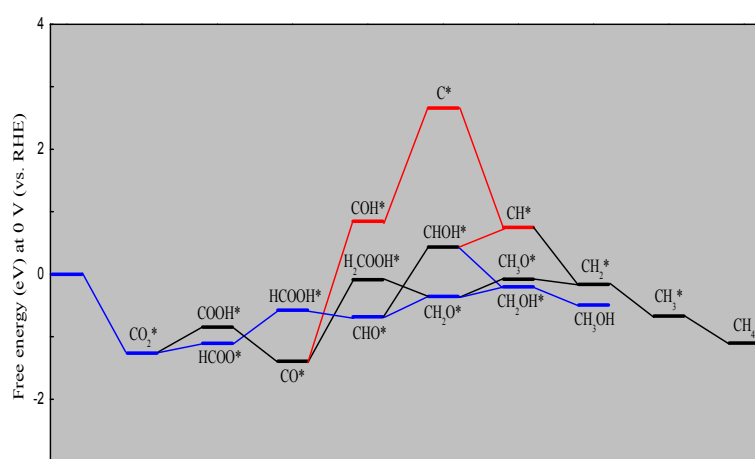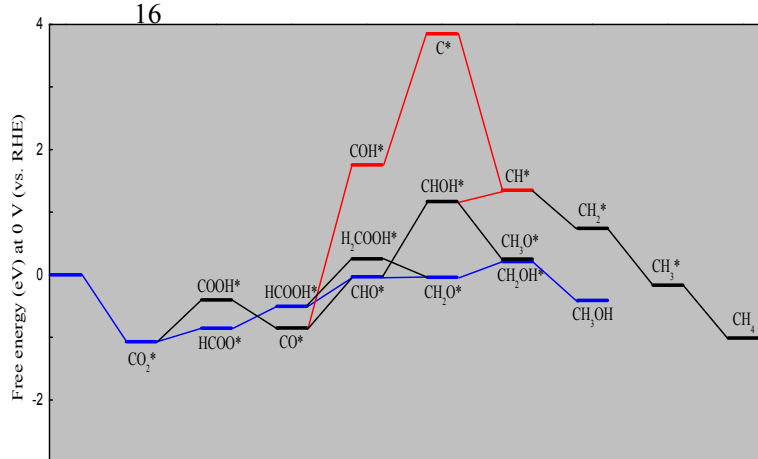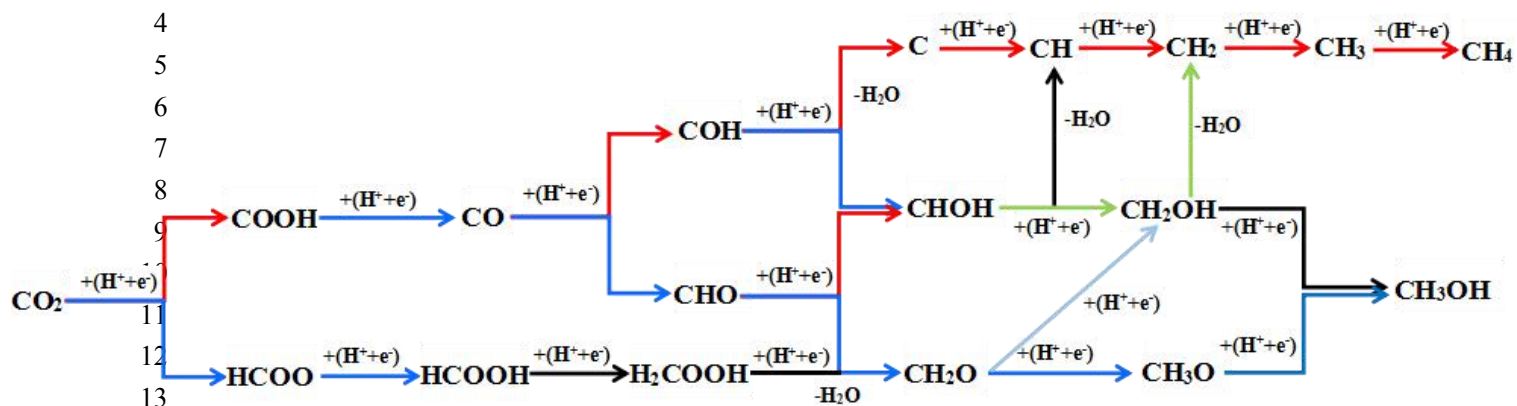
Figure 1. Free energy diagrams for CO_2 reduction on $Pd_{10}Sn_5$ on the Gas-Phase (1) and Solvation

pathway (3) at 0 V (RHE), and on $Pd_{10}Ag_5$ on the Gas-Phase (2) and Solvation pathway (4) at 0 V
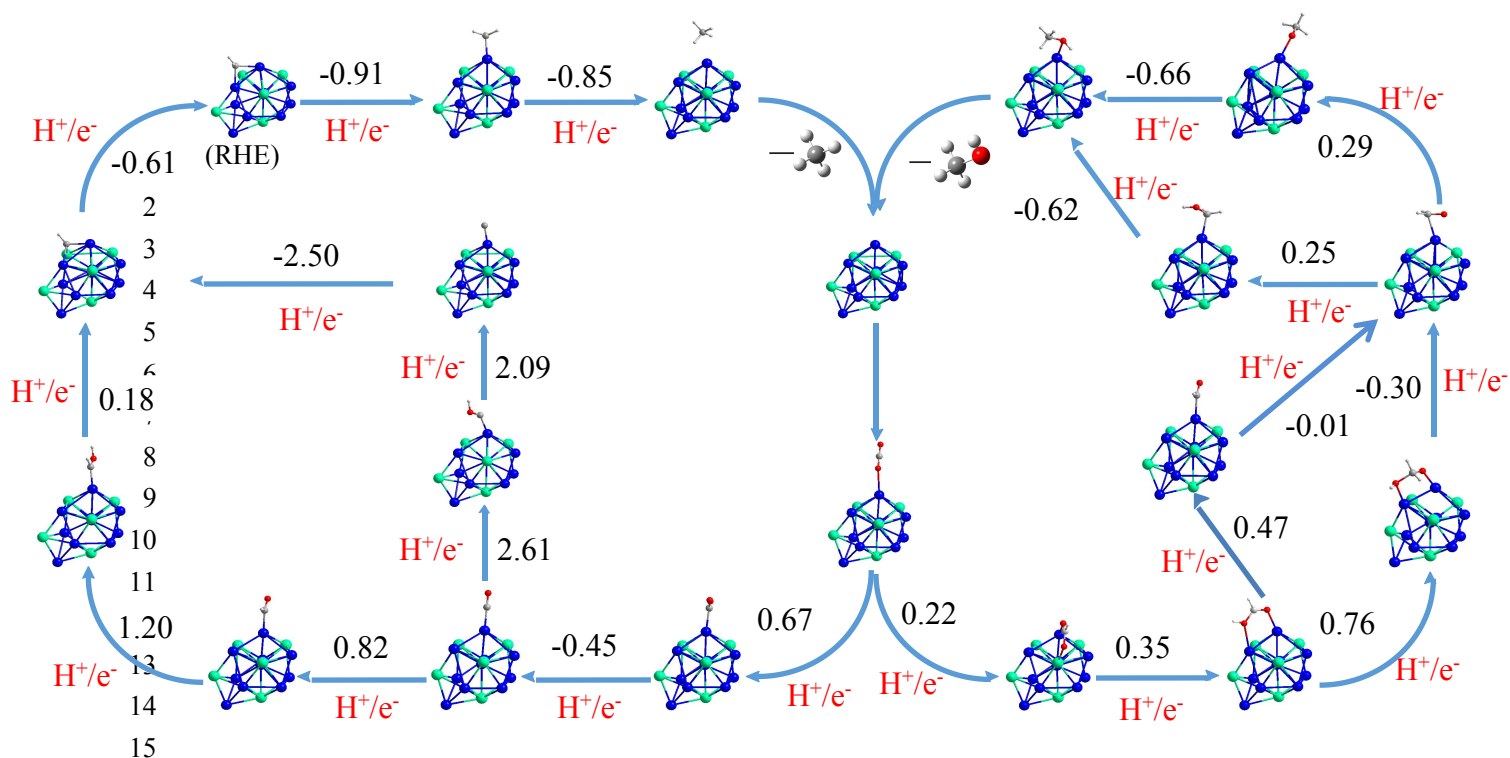
Figure 2. Pathways in the electroreduction of carbon dioxide to CH_3OH or CH_4 on $Pd_{10}Sn_5$. The number around each column corresponds to the relative transfer of proton-electron pairs in response to Gibbs free energy. Pd atoms are in blue, Sn atoms in green, O atoms in red, H atoms in white, and C atoms in gray.
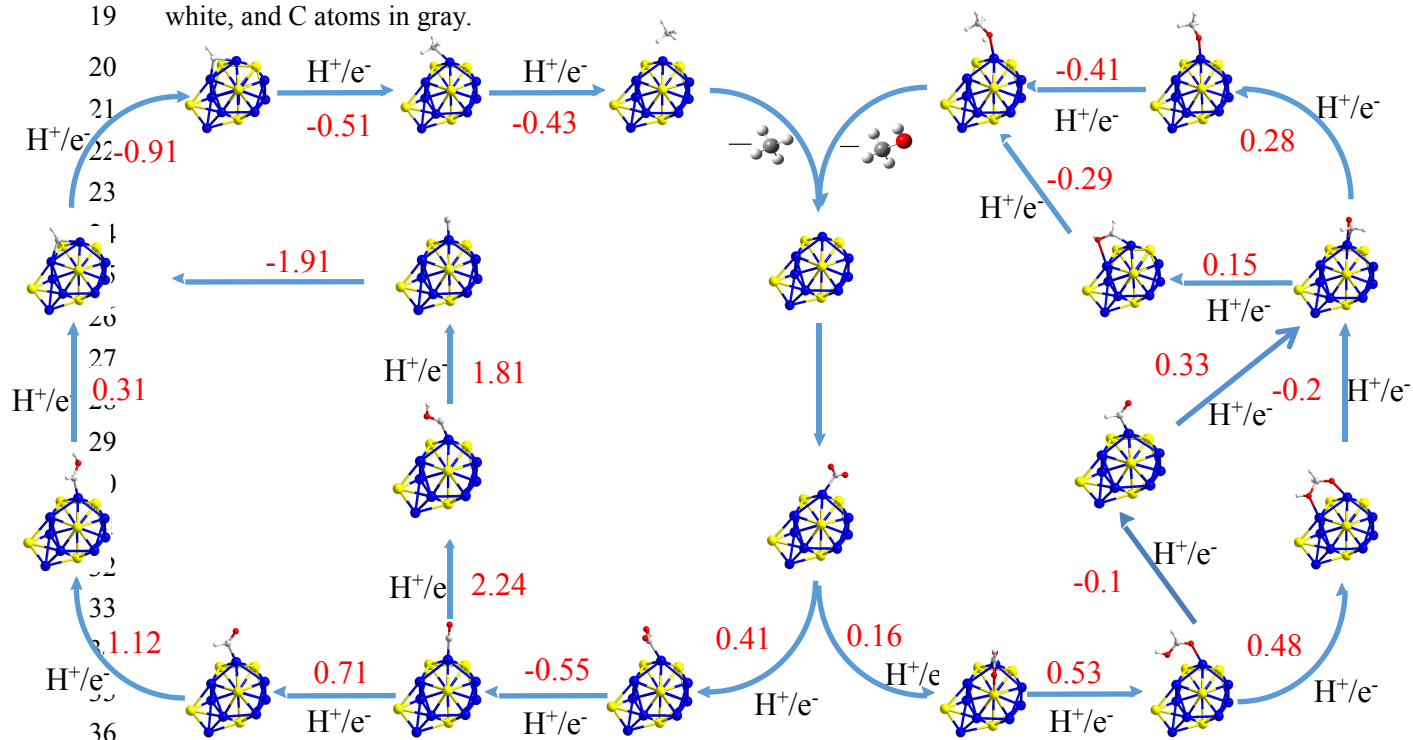

Figure 3. Pathways in the electroreduction of carbon dioxide to CH_3OH or CH_4 on $Pd_{10}Ag_5$. The number around each column corresponds to the relative transfer of proton-electron pairs in response to Gibbs free energy. Pd atoms are in blue, Ag atoms in yellow, O atoms in red, H atoms in white, and C atoms in gray.

1

2 Figure 4. Pathways in the electroreduction of carbon dioxide to C_2H_5OH on $Pd_{10}Sn_5$. The number

3 around each column corresponds to the relative transfer of proton-electron pairs in response to

4 Gibbs free energy. Pd atoms are in blue, Sn atoms in green, O atoms in red, H atoms in white, and

5 C atoms in gray.

6
7
8
9
10
11
12
13
14
15
16
17
18
19
20
21
22
23
24
25
26
27
28
29
30
31
32
33
34
35
36
37
38
39
40
41
42
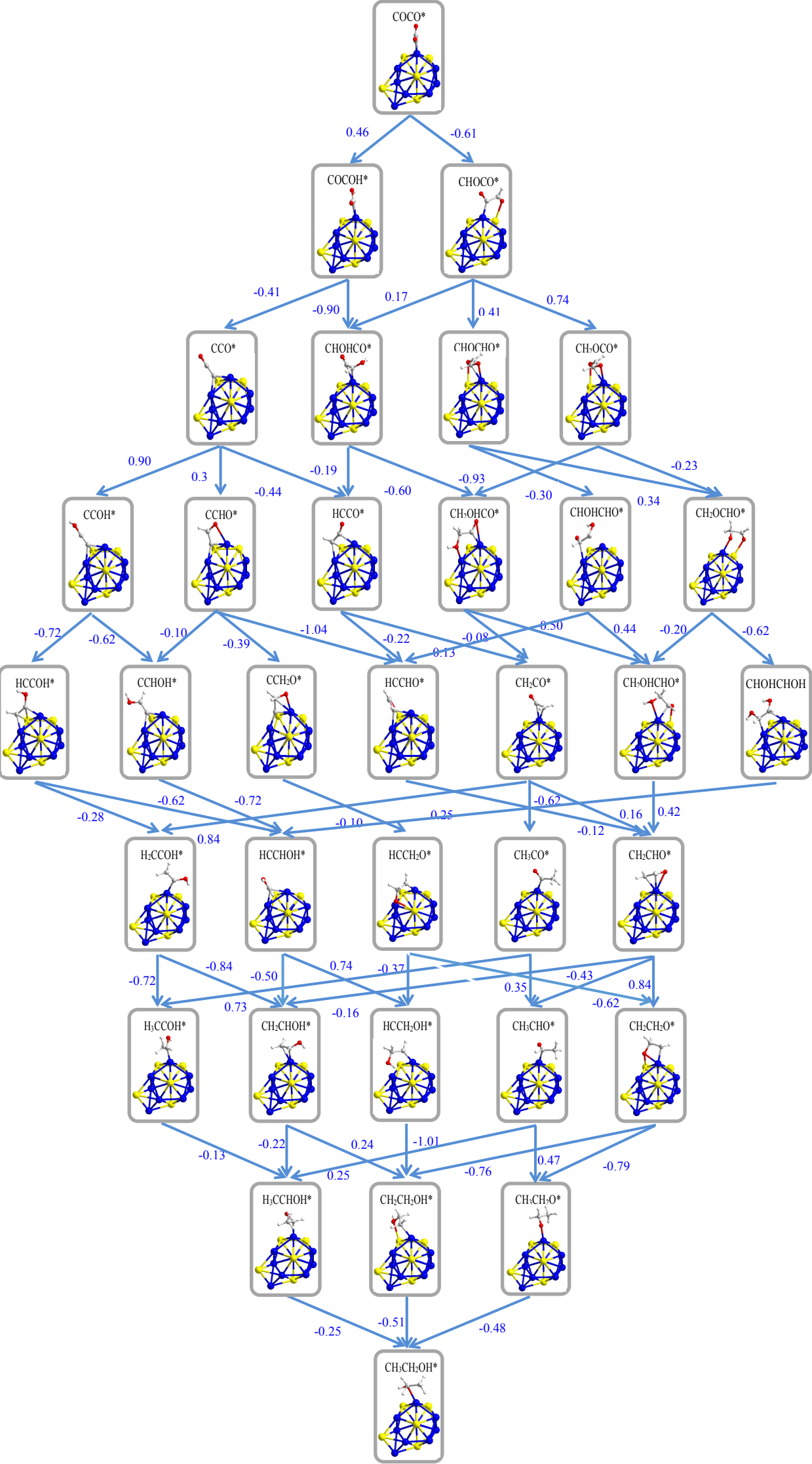
Figure 5. Pathways in the electroreduction of carbon dioxide on $Pd_{10}Ag_5$. The number around each column corresponds to the relative transfer of proton-electron pairs in response to Gibbs free energy. Pd atoms are in blue, Ag atoms in yellow, O atoms in red, H atoms in white, and C atoms in gray.
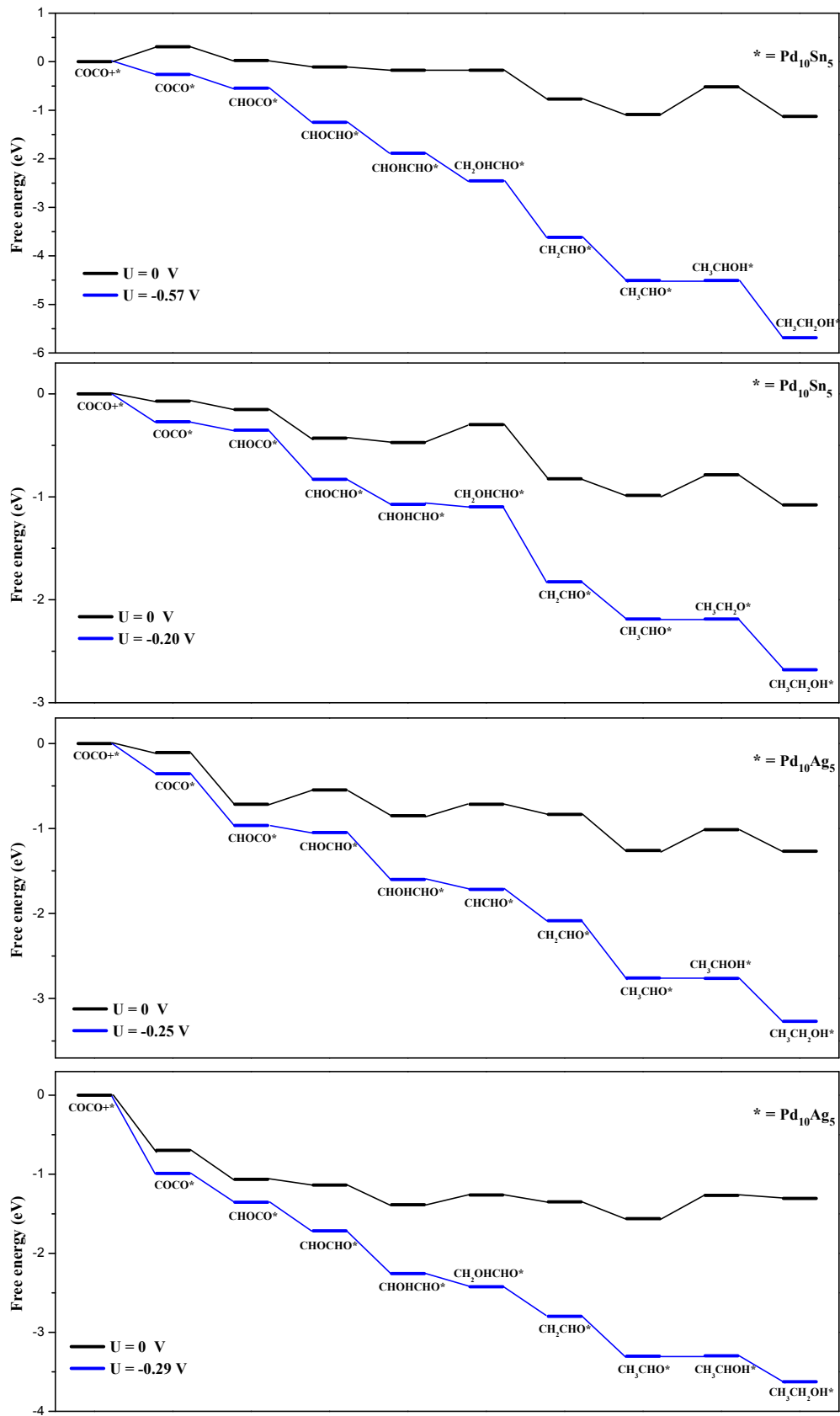
Figure 6. Free energy diagram of the CO₂ reduction pathway to CH₃CH₂OH.
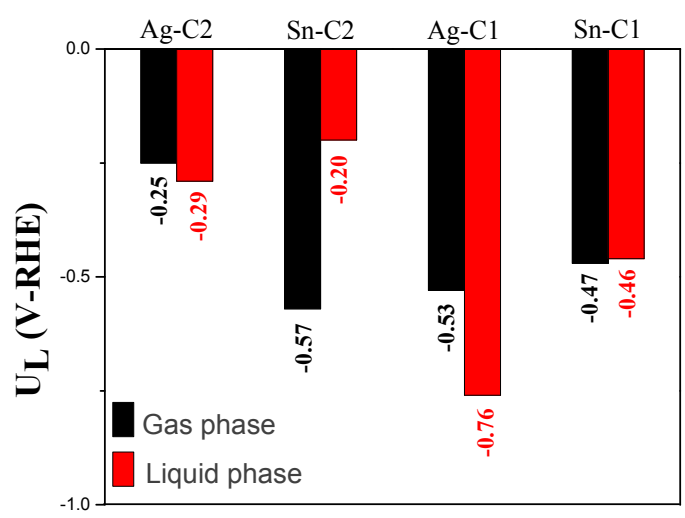
Figure 7. Energy difference in the gas phase and liquid phase for the CO_2 electroreduction selectivity-determining step as a function of the rate-determining step (RDS) reaction energy at zero electrode potential, where the numbers are the energies related to the reactants in eV.

Table 1. The related reactions and the representation of the corresponding rate constant about the CO_2 reduction pathway to CH_3OH.

Reaction	Rate constant	The value [k (s^{-1})] $Pd_{10}Sn_5$ Gas-Phase	The value [k (s^{-1})] $Pd_{10}Sn_5$ Solvation	The value [k (s^{-1})] $Pd_{10}Ag_5$ Gas-Phase	The value [k (s^{-1})] $Pd_{10}Ag_5$ Solvation
$CO_2^*+H^++e^-\rightarrow HCOO^*$	k_1	1.01×10^3	5.78×10^3	3.13×10^2	1.02×10^{-3}
$HCOO^*+H^++e^-\rightarrow HCOOH$	k_2	7.23×10^4	2.06×10^1	2.36×10^{-1}	8.04×10^1
$HCOOH^*+H^++e^-\rightarrow CHO^*$	k_3	7.81	1.15×10^1	5.96×10^4	3.54×10^{-7}
$CHO^*+H^++e^-\rightarrow CH_2O^*$	k_4	8.79×10^4	2.32×10^5	1.15×10^1	4.84×10^{-3}
$CH_2O^*+H^++e^-\rightarrow CH_2OH^*$	k_5	5.62×10^2		3.81×10^2	1.89×10^{-2}
$CH_2OH^*+H^++e^-\rightarrow CH_3OH^*$	k_6	1.24×10^{10}		1.97×10^6	7.58×10^{-1}
$CH_2O^*+H^++e^-\rightarrow CH_3O^*$	k_5		8.53×10^3		
$CH_3O^*+H^++e^-\rightarrow CH_3OH^*$	k_6		3.63×10^7		

Table 2. The related reactions and the representation of the corresponding rate constant about the CO_2 reduction pathway to CH_3CH_2OH.

Reaction	Rate constant	The value [i (s^{-1})] $Pd_{10}Sn_5$ Gas-Phase	The value [i (s^{-1})] $Pd_{10}Sn_5$ Solvation	The value [i (s^{-1})] $Pd_{10}Ag_5$ Gas-Phase	The value [i (s^{-1})] $Pd_{10}Ag_5$ Solvation
$COCO^*+H^++e^-\rightarrow CHOCO^*$	i_1	3.82×10^5	1.27×10^{10}	5.14×10^{13}	9.64×10^{10}
$CHOCO^*+H^++e^-\rightarrow CHOCHO^*$	i_2	1.97×10^4	5.72×10^{11}	1.45×10^7	3.21×10^8
$CHOCHO^*+H^++e^-\rightarrow CHOHCHO^*$	i_3	5.54×10^3	6.00×10^9	1.34×10^{11}	1.02×10^{10}
$CHOHCHO^*+H^++e^-\rightarrow CH_2OHCHO^*$	i_4	1.47×10^3	8.77×10^7	2.75×10^7	7.14×10^6
$CH_2OHCHO^*+H^++e^-\rightarrow CH_2CHO^*$	i_5	1.50×10^8	7.37×10^{13}	3.71×10^9	4.16×10^8
$CH_2CHO^*+H^++e^-\rightarrow CH_3CHO^*$	i_6	6.97×10^5	5.99×10^{10}	1.47×10^{12}	5.07×10^9
$CH_3CHO^*+H^++e^-\rightarrow CH_3CHOH^*$	i_7	2.40×10^{-2}	5.39×10^7	3.09×10^6	2.60×10^5
$CH_3CHOH^*+H^++e^-\rightarrow CH_3CH_2OH^*$	i_8	2.02×10^8	7.67×10^{11}	5.31×10^{10}	1.62×10^8